Departamento de Biología Celular
Universidad de Barcelona

Sexual reproduction in demosponges: ecological and evolutive implications

Reproducción sexual en demosponjas: implicaciones ecológicas y evolutivas

Ana Riesgo Gil

Barcelona 2007

Chapter 5:

Introduction

According to what is found in many lower invertebrates, the archetype of "classical primitive" sperm (*sensu* Franzén 1996; Reunov 2005) is usually regarded to be a flagellated round cell ontogenetically derived from a flagellated spermatogonium, and bearing proacrosomal vesicles rather than a true acrosome. Such sperms occurs typically associated to truly external fertilization (i.e., ectaquasperms, *sensu* Rouse and Jamieson 1987) in many lower invertebrates, so that such structural and functional features are widely postulated to represent the ancestral condition in at least Eumetazoa, i.e., Metazoa after excluding Porifera and Placozoa (Franzén 1956; Afzelius 1972, 1979; Baccetti and Afzelius 1976; Reunov 2001). Caution when referring to the Porifera emerges from the fact that, although this group posses many features that are widely considered ancestral in the metazoan linage, some of its members also show a handful of "puzzling" reproductive traits that strongly conflict with the ancestral status attributed to the group. For instance, many poriferans do not exhibit external fertilization -the ancestral condition of sexual reproduction- but are sperm-casters (*sensu* Bishop and Pemberton 2006) with internal fertilization followed by brooding and true viviparism of maternally-fed embryos (e.g., Fell 1974; Maldonado and Bergquist 2002; Maldonado 2006). Furthermore, internal fertilization in the Porifera is thought to be mediated by choanocytes and carrier cells that exhibit complex cell behaviors, including oriented migration and specific cell recognition of spermatozoa and oocytes (e.g., Fell 1974; Simpson 1984; Harrison and De Vos 1991; Nakamura et al. 1998).

Among the Porifera, demosponges are the best studied group regarding spermatogenesis and sperm structure (reviews: Tuzet 1964; Reiswig 1983; Boury-

Esnault and Jamieson 1999). In most cases, spermatogonia have been reported to derive from choanocytes, a somatic, flagellated cell line that makes the internal feeding epithelia. This origin has been reported for species in many demosponge groups, such as Homosclerophorida (Lévi 1956; Tuzet and Paris 1964; Gaino et al. 1986; Boury-Esnault and Jamieson 1999), Astrophorida (Scalera-Liaci and Sciscioli 1969, 1970), Hadromerida (Diaz and Connes 1980), Chondrosida (Usher et al. 2004), Halichondrida (Barthel and Detmer 1990), Haplosclerida (e.g., Tuzet 1932; Leveaux 1942; Paulus 1989), Dendroceratida (Tuzet et al. 1970), and Dictyoceratida (Tuzet and Pavans de Ceccatty 1958; Gaino et al. 1984; Kaye and Reiswig 1991). Alternatively, spermatogonia have been postulated to derive from unflagellated, totipotent, amoeboid cells of the sponge mesohyl, the archaeocytes. This has been the case for the haplosclerid *Reniera simulans* (Tuzet 1930b), the halichondriid *Hymeniacidon heliophila* (Fincher 1940), halisarcids as *Halisarca* (Lévi 1956), the hadromerids *Tethya aurantium* and *Polymastia mamillaris* (Lévi 1956), as well as the poecilosclerid *Neofibularia nolitangere* (Hoppe and Reichert 1987) and *Latrunculia* spp. (Ilan 1995). Additionally, archaeocytes are proposed to be the origin of spermatogonia in all choanocyte-lacking, carnivorous, cladorhizid poecilosclerids (Boury-Esnault and Jamieson 1999). Finally, spermatogonia are suggested to derive from mesohyl storage cells in the agelasid "sclerosponge" *Goreauiella auriculata* (e.g., Willenz and Hartman 2004). Therefore, the spermatogonia of demosponges have an atypical, variable origin when compared to that of other animals.

A few demosponge species, distributed across different groups, show the expected "classical primitive sperm" (*sensu* Franzén 1996; Reunov 2005*)*, i.e., a round cell with abundant cytoplasm and bearing a flagellum at the posterior (in the sense of movement) cell pole. This is the case for several species of *Chondrilla* (e.g., Usher et al. 2004; Maldonado, personal communication), *Agelas sceptrum* (Reiswig 1983), *Verongia archeri* (Reiswig 1970), and 2 species of *Aplysilla* (Schulze 1878; Tuzet et al. 1970). It was first thought that the absence of acrosome was the rule in sponge sperms. Nevertheless, proacrosomal vesicles, usually regarded to represent the evolutionary step previous to the apparition of the acrosome (e.g., Baccetti 1979; Franzén 1996), have been found in the hadromerid *Suberites massa* (Diaz and Connes 1980) and the Dictyoceratid *Spongia officinalis* (Gaino et al. 1984). Some early studies based on optical microscopy vindicated the occurrence of a real acrosome in some demosponges,

such as *Geodia* sp. (Reiswig 1970) and *Hippospongia communis* (Tuzet 1964). Using electron microscopy, an acrosome has been demonstrated to occur in all studied homosclerophorid demosponges (Bacetti et al. 1986; Boury-Esnault and Jamieson 1999; Riesgo et al. 2007). A large, conical acrosome has also been reported in the sperm of some calcareous sponges (Tuzet 1947; Nakamura et al. 1998). Consequently, in contrast to the view that primitive sperms may have arisen independently in the Porifera and Eumetazoa (Afzelius 1972; Franzén 1996), it has now been suggested that the spermatozoon is homologous in all Metazoa (e.g., Mohri et al. 1995) and that the absence of acrosome in most sponges may be a derived condition (Baccetti et al. 1986; Harrison and De Vos 1991; Boury-Esnault and Jamieson 1999; Riesgo et al. 2007). Boury-Esnault and Jamieson (1999) also stressed that the spermatozoon structure in several demosponges, such as *Ephydatia fluviatilis, Lubomirskia baikalensis, S. officinalis*, and *Aplysilla rosea*, share some traits with the "aberrant aquasperm" of some teleost fish, which is considered to be secondarily simplified (Jamieson 1991). In addition, cone-shaped and relatively lengthened sperms, which depart from the archetype of classical primitive sperm (*sensu* Reunov 2005), have been reported in members of various demosponge groups, such as some *Halisarca* species, *S. massa*, *H. heliophila*, *Microciona atrasanguinea*, and *H. communis* (reviewed by Reiswig 1983; Boury-Esnault and Jamieson 1999). A bizarre V-shaped spermatozoon has also been described in the halichondrid *Halichondria panicea* (Barthel and Detmer 1990). Yet, the most atypical spermatozoon known in demosponges so far belongs to the poecilosclerid *Crambe crambe*. It shows V-shaped morphology and a flagellum inserted within a deep cytoplasmic pit (Tripepi et al. 1984). Unfortunately, the description of this distinct sperm is based on just a very brief report included in the Abstracts book of the 8th European Congress of Electron Microscopy. As it was noticed by Boury-Esnault and Jamieson (1999) in their review of the poriferan sperms, many of the peculiar ultrastructural traits mentioned by Tripepi and co-workers (1984) remain intriguing in the brief original description and need further investigation. In this study, we have revisited the sperm of *C. crambe* in an attempt to obtain new ultrastructural information for a better understanding of both its distinctive cytological organization and the spermatogenetic process that leads to such unconventional morphology.

Material and methods

Sampling

We studied a population of the hermaphroditic demosponge *Crambe crambe* (Schmidt 1862), a dominating, encrusting organism in the sublittoral rocky communities of northeastern Mediterranean coast of Spain (e.g., Maldonado et al. 2005). To conduct a general monitoring of reproductive activity in the population, we tagged 5 large and presumably mature individuals, which were sampled monthly, from October ´03 to October ´05. Using scuba and surgical scissors, we collected a small tissue piece (approx. 1 x 0.5 x 0.3 cm) from each sponge at each sampling time. In any case tissue collection involved dead or perceptible signs of illness in the injured sponges over the study period. During the first year of study, when samples from the tagged individuals revealed that gametogenetic activity was peaking in the population, which happened from late spring to mid summer, we increased both number of tagged individuals (25 individuals) and sampling frequency (approx. 10-day intervals).

Light microscopy

Tissue samples for light microscopy were maintained in ambient seawater for transportation to the laboratory and fixed within 2 h after collection in 4% formaldehyde in seawater for 24 h. Then, samples were desilicified with 5% hydrofluoric acid for 1.5 h, rinsed in distilled water, dehydrated through a graded ethanol series, cleared in toluene, and embedded in paraffin to cut them into 5 μm-thick sections with an Autocut Reichert-Jung microtome 2040. After deparaffining with xylene, sections were stained with Hematoxylin-PAS, and studied through a Zeiss Axioplan II compound microscopy connected to a Spot Cooled Color digital camera. We estimated the number of cyst-producing sponges in the population overtime by taking 2 pictures (6.96mm^2) of each of 2 non-serial histological sections per individual and sampling time. Pictures were taken at least 240 μm from each other to avoid overestimation due to overlapping of cysts. Then, we used the public domain ImageJ Software (http://rsb.info.nih.gov/ij/index.html) on the digital histological images to estimate percentage of tissue occupation by cysts, measuring maximum diameter and cyst area per area unit of tissue

in the reproductive individuals. Though cysts are usually subspherical structures, such measurements provide only a relatively approximate assessment of tissue occupancy because all cysts in a section are not caught at their maximum diameter. Nevertheless, because we studied a total of about 550 sections, we assumed that parametric statistics works and that measured mean values are reliable, though affected by a large (non-natural) standard deviation (SD) artificially increased by position of sections in the cyst.

Transmission electron microscopy

The ultrastructure of spermatogenesis was documented using transmission electron microscopy (TEM). The protocol is detailed in Chapter 2.

Results

Dynamics of cyst production

We examined histological sections of a total of 80 individuals during the 2-year monitoring (October, 2003 to September, 2005). In this hermaphroditic sponge, spermatic cysts occurred in about 50-60% of individuals in the population (Fig. 1A) for about 3 months each year, from late spring to early summer.

During 2004, cysts appeared in May, but they did it one month earlier (April) the following year. In both years, cysts appeared abruptly in the sponges, coincidentally with the seasonal rising of seawater temperature (Fig. 1a). In contrast, they disappeared gradually during summer (Fig.1A). Cyst size did not change substantially over the reproductive period, with average maximum diameter per month ranging from 49.18±36.02 µm to 65.94±56.46 µm during 2004 and from 46.34±9.05 µm to 78.76±46.55 µm during 2005 (Fig. 1B).

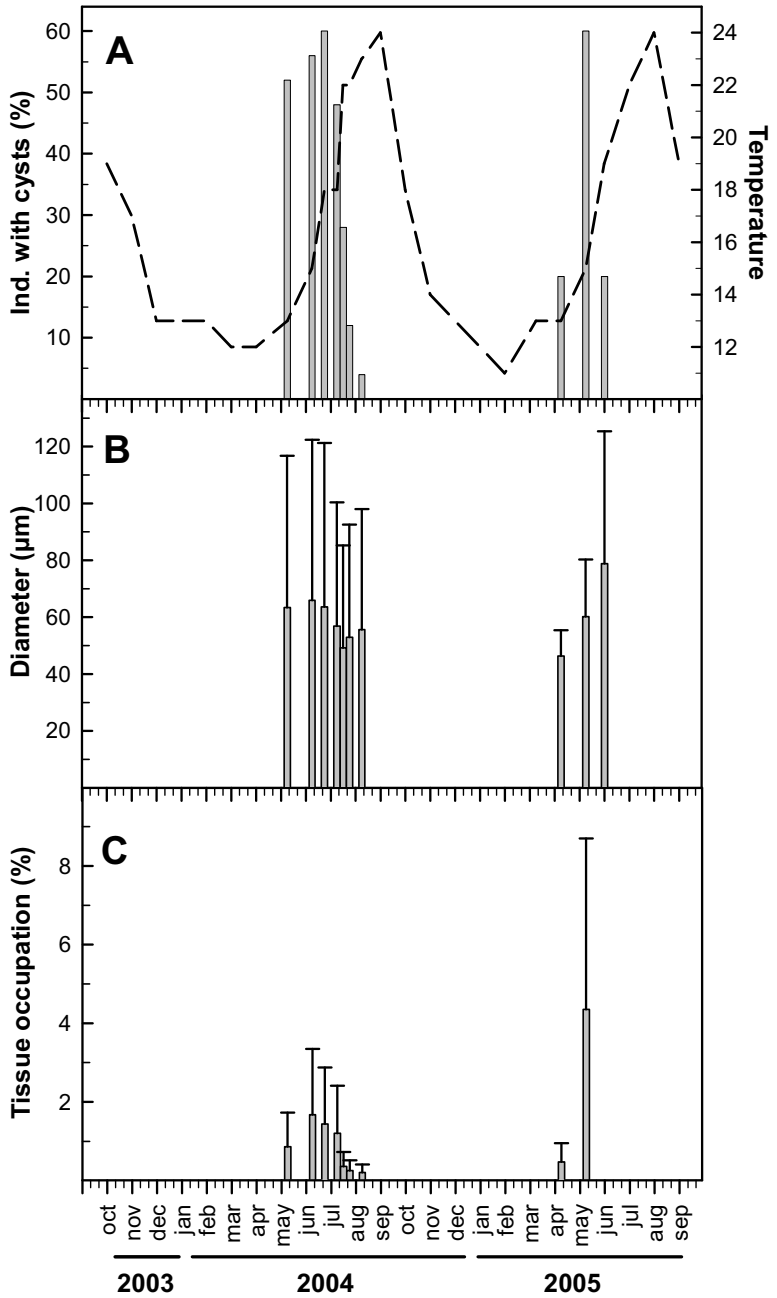

Figure 1. Dynamics of spermatogenesis over a 2-year period. **(A)** Percentage of individuals engaged in spermatic cyst production in the population over time plotted versus seawater temperature. **(B)** Time dynamics of cyst size (mean ± standard deviation). **(C)** Tissue occupation (%) by cysts. Number of individuals sampled and sampling frequency increased from 5 to 25 ind. and from 1-month to 10-day intervals, respectively, in summer, 2004.

Tissue occupation by cysts over the spermatogenic cycle was 1.70 % on average. The highest values occurred in June (0.98 %) during 2004 and in May (5.53 %) during 2005, with sponges making a much higher investment in cyst production per area unit of tissue the latter year (Fig.1C). Each year, we detected some individuals with quite high cyst production (4 to10 % of tissue occupation), individuals with low production (<0.01 %), and individuals showing no reproductive activity at all. Individuals with high production in 2004 did not necessarily have high production in 2005 and vice versa. Tagged individuals that did not reproduce in 2004, neither did it the following year.

Ultrastructure of cysts formation

The spermatic cysts appeared to derive from choanocyte chambers, as revealed by direct observations of choanocytes that doubled their nuclear (mean diameter: 4.15 µm) and cell (6.12 µm in mean height and 5.76 µm in mean width) size, were losing their collar, and leaving the chambers (Fig. 2A). Prior to transdifferentiation, choanocytes measured 3.5 µm on average height and 3.2 µm on average width. Groups of migrated choanocytes appeared to re-aggregate in the mesohyl and were rapidly enveloped by a cellular follicle of unascertained origin (Fig. 2A, 3A). The epithelium-like follicle was built by flattened cells with a prominent round nucleus, which were connected by interdigitate junctions (Fig. 2B-C, 3C, 4A).

First cysts appeared in the mesohyl region close to the basopinacoderm, while late cysts occupied the remaining upper mesohyl regions, intermingled with choanochambers. Each cyst often contained cells in the same stage of spermatogenesis, i.e., within-cyst synchronous development (Figs. 3A, 4A, 5A). However, there was between-cyst asynchrony, with adjacent cysts often being in different stages of development (Fig. 3C).

Ultrastructure of spermatogonia and primary spermatocytes

Early-stage cysts were densely packed with cells, usually consisting of both spermatogonia and primary spermatocytes (Fig. 3A). It was hard to discern between spermatogonia and primary spermatocytes because of their similar features. Both were round cells (about 5 µm in diameter), showing a large nucleus (4 to 4.5µm in diameter),

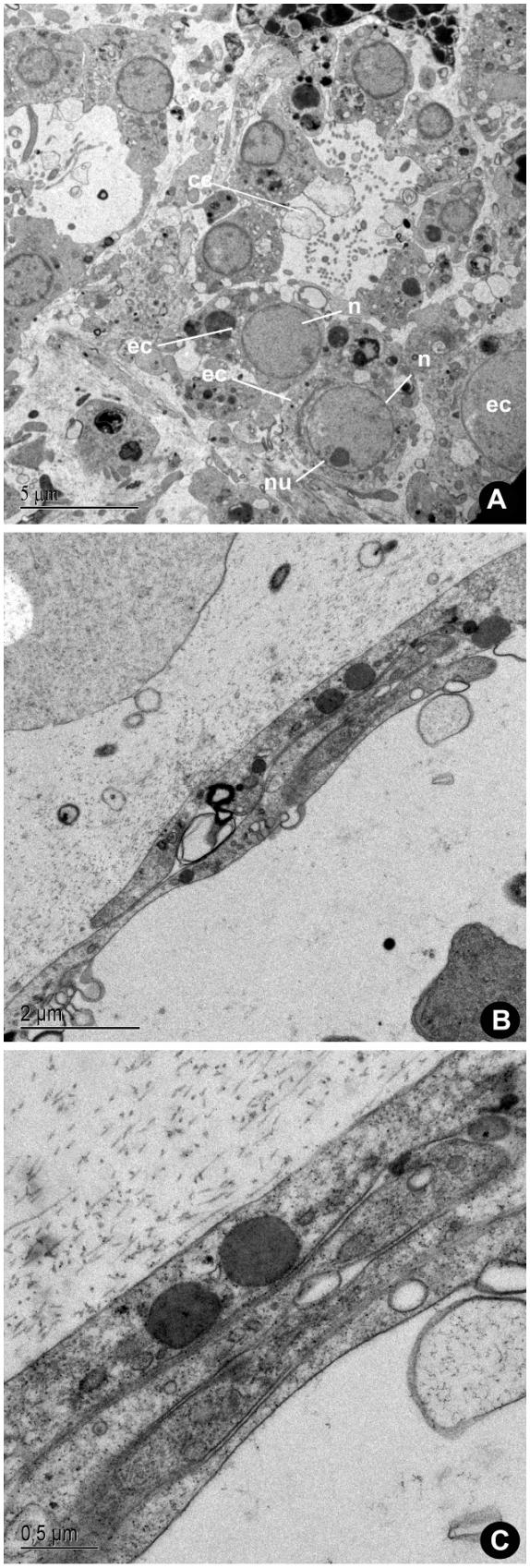

Figure 2. Early spermatogenesis stages. **(A)** Choanocyte chamber showing a transition gradient from "regular" choanocytes to abnormally large choanocytes (ec) with swollen nuclei (n), which are leaving the chamber (cc) to become spermatogonia. Note the nucleolus (nu) in one of the enlarged choanocytes. **(B-C)** Interdigitate junctions in the cellular follicle of the spermatic cyst.

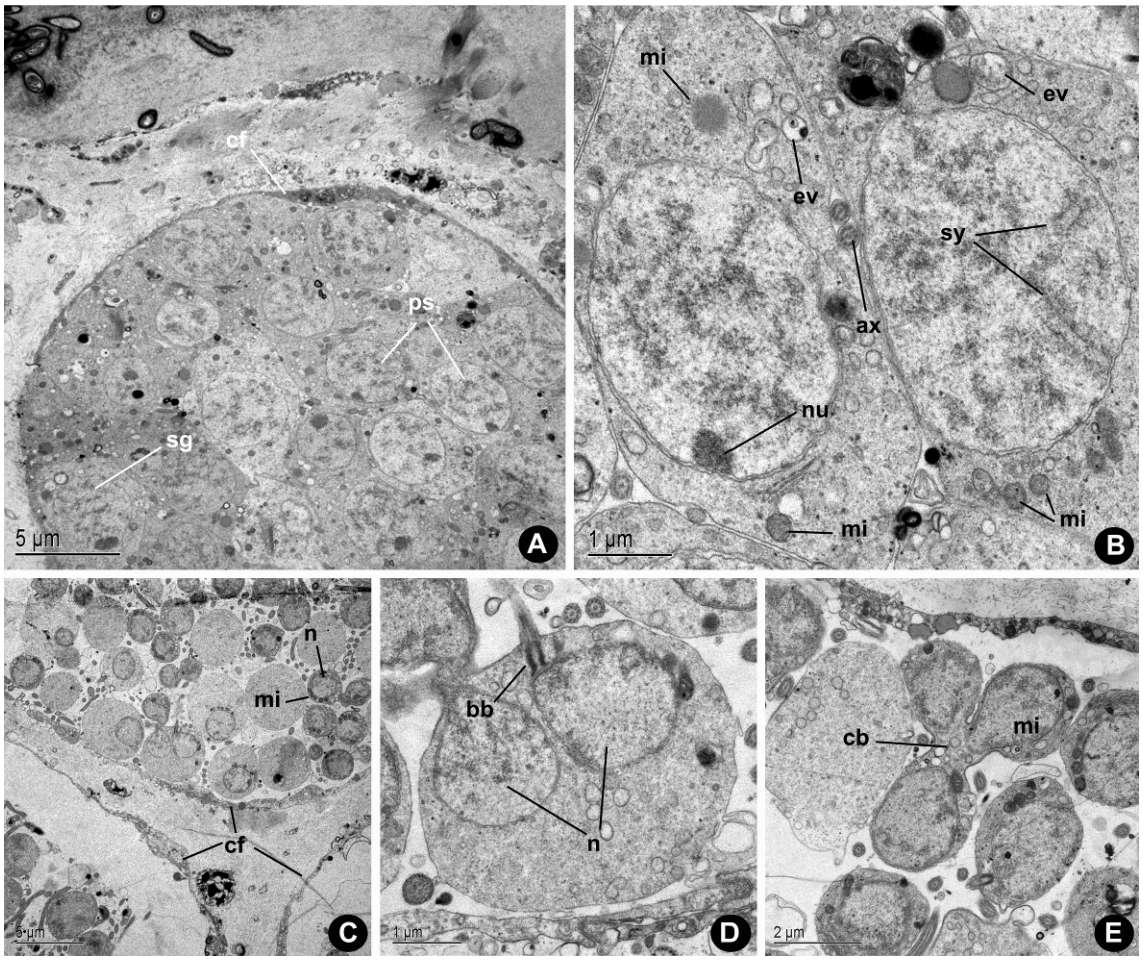

Figure 3. Spermatogonia and primary spermatocytes. **(A)** Spermatic cyst containing both spermatogonia (sg) and primary spermatocytes (ps). A cellular follicle (cf) envelops the cyst. **(B)** A spermatogonium (to the right) showing a nucleolate nucleus (n) and a primary spermatocyte with synaptonemal complexes (sy). The cytoplasm of both cells contains several mitochondria (mi) and electron-clear vesicles (ev). Cross sections of axonemes (ax) occur intercellularly in the cyst. **(C)** Three adjacent spermatic cysts containing primary spermatocytes (ps) and enveloped by a cellular follicle (cf). Late primary spermatocytes show a reduced nucleus (n) compared to earlier stages, also an ordered arrangement of the mitochondria (mi). **(D)** Primary spermatocyte approaching the cytokinesis of the first meiotic division, in which 2 nuclei (n), the basal body (bb) and the tail are seen. **(E)** Primary spermatocytes interconnected by a cytoplasmic bridge (cb). Note the arrangement of mitochondria (mi) around the nuclei.

the Golgi apparatus, mitochondria with well-defined, flattened cristae, and several inclusions and electron-clear vacuoles of uncertain nature (Fig. 3A).

Nevertheless, spermatogonia were distinguishable from spermatocytes by having a large nucleolus within the nucleus (Fig. 3A). We documented the flagellum insertion in various TEM sections of primary spermatocytes (Fig. 3D), but such equivalent sections were not found for spermatogonia. Anyway, given the high number of cilia observed in general sections of early stage cysts, we believe that these choanocyte-derived spermatogonia were also flagellated cells with basal body and accessory centriole.

Figure 4. Secondary spermatocytes. **(A)** Spermatic cyst containing secondary spermatocytes (ss) with incipient condensation of chromatin in their nucleus (n), and limited by a cellular follicle (cf). Note production of cytoplasmic drops (cy) resulting from the cytoplasmic reduction of the first meiotic division. **(B-D)** Secondary spermatocytes showing a peripheral, "nucleolus-like" condensation of chromatin (nc) in the nucleus (n), the basal body (bb), the accessory centriole (ac), some electron-clear vesicles (ec), mitochondria (mi), and a Golgi apparatus (g). Cytoplasmic bridges (cb) interconnect sister cells. **(E)** Nucleus of a secondary spermatocyte showing tube-like structures (ts) at the inner nuclear membrane (nm). A well developed Golgi apparatus (g) starts producing the vesicles (gv) that will originate the acrosome. **(F)** Close-up of a spermatocyte's nucleus showing the intranuclear tube-like structures (ts) and the highly ordered arrangement of mitochondria (mi) around the nuclear envelope.

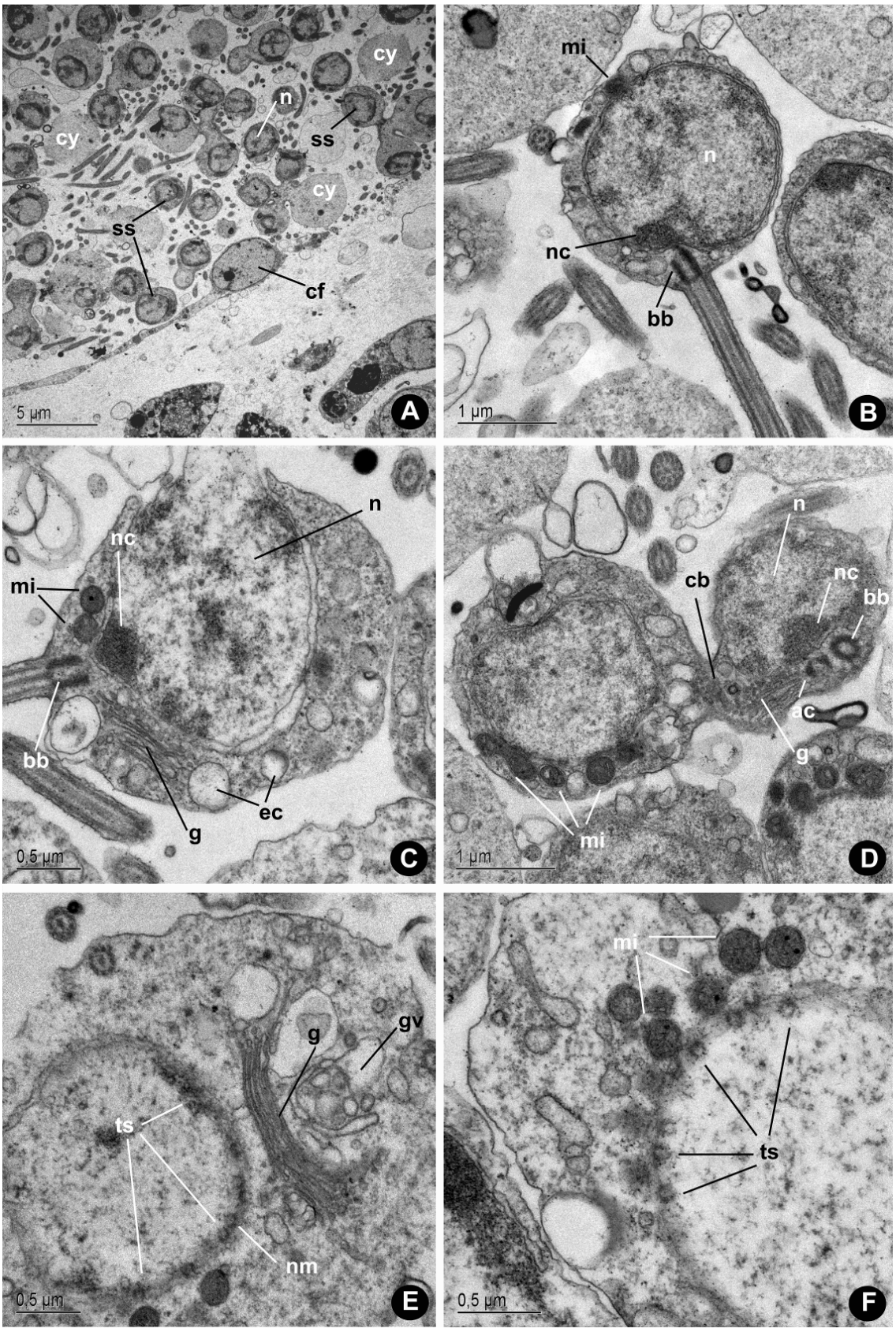
cy
n
ss
cy
cy
ss
cf
5 µm
A
mi
n
nc
bb
1 µm
B
n
nc
mi
bb
g
ec
0,5 µm
C
n
cb
nc
bb
ac
g
mi
1 µm
D
g
gv
ts
nm
0,5 µm
E
mi
ts
0,5 µm
F

Unlike spermatogonia, primary spermatocytes showed developed synaptonemal complexes, indicating that they were engaged in prophase I (Figs. 3A-B). As spermatogenesis advances cysts became laxer, with primary spermatocytes clearly outnumbering spermatogonia. Primary spermatocytes started reducing their nuclear size (Fig. 3C-D), then also their cell size by exocytosing part of the cytoplasm (Fig. 3e). At this late stage, several small round mitochondria occurred in a highly ordered distribution around the nucleus (Fig. 3C, E). After experiencing nuclear division (Fig. 3D), late-stage primary spermatocytes underwent incomplete cytokinesis, with daughter cells (i.e., secondary spermatocytes) remaining interconnected by cytoplasmic bridges (Fig. 3E).

Ultrastructure of secondary spermatocytes

Secondary spermatocytes were round, flagellated cells, about 2.5 µm in diameter (Fig. 4b). They engaged in a process of chromatin condensation, which started at the inner side of the nuclear membrane and became particularly evident at the area adjacent to the flagellum insertion, where a transient nucleolus-like structure appeared (Fig. 4B-D). At the tail insertion, the basal body of the flagellum and a perpendicular accessory centriole were patent (Fig. 4B-D). The cytoplasm contained electron-clear vacuoles and a well developed Golgi apparatus (Fig. 4C-E). The small mitochondria maintained their ordered arrangement around the nuclear membrane (Fig. 4D, F). Interestingly, several small, electron-dense tube-like structures appeared at the internal side of the nuclear membrane, just in front of the mitochondria (Fig. 4E-F). While experiencing the second meiotic division, secondary spermatocytes exocytosed most of their cytoplasm in the form of large electron-clear drops (Fig. 5A-B). As a result, the cyst appearance became quite lax.

Ultrastructure of spermatids

Spermatids exhibited a drastic change in morphology relative to spermatocyte stages. They became lengthened cells, being 5.5 µm long and 1.7 µm wide on average. The nucleus stretched along the longitudinal axis, achieving a length of up to 4.5 µm and narrowing up to 0.5 µm in width (Fig. 5C). Chromatin experienced a peculiar process of "multipolar" condensation, forming small, electron-dense clumps ("initiation

centers") which were scattered all over the nucleus (Fig. 5C, F-G). A longitudinal cytoplasmic tunnel, running from the tail insertion (i.e., original posterior cell pole) to the anterior cell pole, was formed to harbour the proximal region of the axoneme (Fig. 5D, F). Therefore, the flagellum bent at a 180º angle (Fig. 5D-F). As a result, the cell became V-shaped, with the flagellum becoming free for beating near the original anterior pole of the spermatid (Fig. 5F), which apparently turned into the new functional posterior pole of the future spermatozoon. The flagellum showed a typical 9+2 microtubule structure, with alar sheets and anchoring points at the transition region between the axoneme and the basal body (Fig. 5L). The accessory centriole was not visible at this stage, having probably been disassembled. The several mitochondria occurring in previous stages fused into a large single mitochondrion that migrated to the cell pole opposite the tail insertion, below the nucleus (Fig. 5C-E). It is also worth noting the formation of striated ciliary rootlets, which originated from a terminal plate of the basal body (Fig. 5K) and extended to contact the mitochondrion located at the opposite cell pole, running between the nuclear membrane and the cytoplasmic tunnel (Fig. 5F-J). In early spermatids, the Golgi apparatus, which located at the original anterior pole adjacent to the newly formed mitochondrion (Fig. 5E), produced a large vesicle (Fig. 5E, J). In late spermatids, this vesicle (pre-acrosomal vesicle) migrated to the new functional anterior pole and began differentiating into an electron-dense acrosomal complex (Fig. 5F, K-L). Microtubules running parallel to the internal side of the plasmalemma in the cytoplasmic bridges between spermatids were also other trait not observed in previous stages (Fig. 5C, J).

Ultrastructure of spermatozoa

We never observed free-swimming spermatozoa, but just nearly mature stages sharing the cysts with spermatids that were still exocytosing part of their cytoplasm (Fig. 5A, 6A). In cysts containing mostly putative mature spermatozoa, intercellular bridges were not observed. Other major difference with spermatids was that the earlier chromatin clumps condensed into a single helical structure in spermatozoa (Fig. 6A-C). These spermatozoa were long and narrow flagellated cells, with cell bodies averaging 6.5 μm in length and 0.6 μm in width (Fig. 6A, C, 7A).

There was neither Golgi apparatus nor accessory centriole. The proximal region of the flagellum ran within a cytoplasmic tunnel (Fig. 6A-D) until about the middle of the cell length, where it became free (Fig. 6A). Interestingly, the axis of the free-beating axoneme appeared to cross the longitudinal axis of the cell body (Fig. 6C, 7A). Like in spermatids, the striated rootlets that originated from the basal body crossed longitudinally the cell to contact the single mitochondrion located at the opposite pole (Fig. 6C).

Figure 5. Spermatids. **(A)** Spermatic cyst limited by a cell follicle (cf) and containing spermatids (s) and mature spermatozoa (sp). Intercellular electron-clear vacuoles result from processing of cytoplasmic drops (cy). **(B)** Spermatids exocytosing large electron-clear vacuoles (ev) with cytoplasm excess. **(C-D)** Spermatids with lengthened nucleus (n) showing multiple "initiation centers" (ic) of chromatin condensation, the cytoplasmic tunnel (ct) lodging the axoneme (ax), and the newly-formed single mitochondrion (mi). Note that sister spermatids (Fig. 5c) are connected by cytoplasmic bridges (cb) reinforced by microtubules (m). **(E)** Detail of the functional posterior pole showing the mitochondrion (mi), the nucleus (n), and a putative "pre-acrosomal" vesicle (gv) produced by the Golgi apparatus (g).**(F-G)** Longitudinal sections of spermatids showing the axoneme (ax), the striated ciliary rootlets (cr), and the nucleus (n) with multiple "initiation centers" (ic). A developing acrosomal complex (a) occurs close to the basal body (bb). **(H)** Spermatid cross-sectioned near the level of the tail insertion showing "initiation centers" (ic) in the nucleus (n), ciliary rootlets (cr) associated with the external nuclear membrane, and the cytoplasmic tunnnel that harbors the axoneme (ax). **i** Spermatid cross-sectioned at its mid length showing the ciliary rootlets (cr) and the free-beating axoneme (ax) before entering the cytoplasmic tunnel.**(J)** Detail of striated ciliary rootlets (cr) in close association with the mitochondrion (mi). Note the migrating "pre-acrosomal vesicle" (pa) and the microtubules (m) reinforcing the plasmalemma at the inter-spermatid bridges. **(K)** Detail of a spermatid showing the insertion of the axoneme (ax), the basal body (bb) with a terminal plate (bp) from which ciliary rootlets (cr) originate, and the conical acrosome (a). **(L)** Cross section of a spermatid at the basal body level in which alar sheets (as) and anchoring points (ap) can be inferred. The incipient acrosomal complex (a) and the nucleus (n) are also seen. →

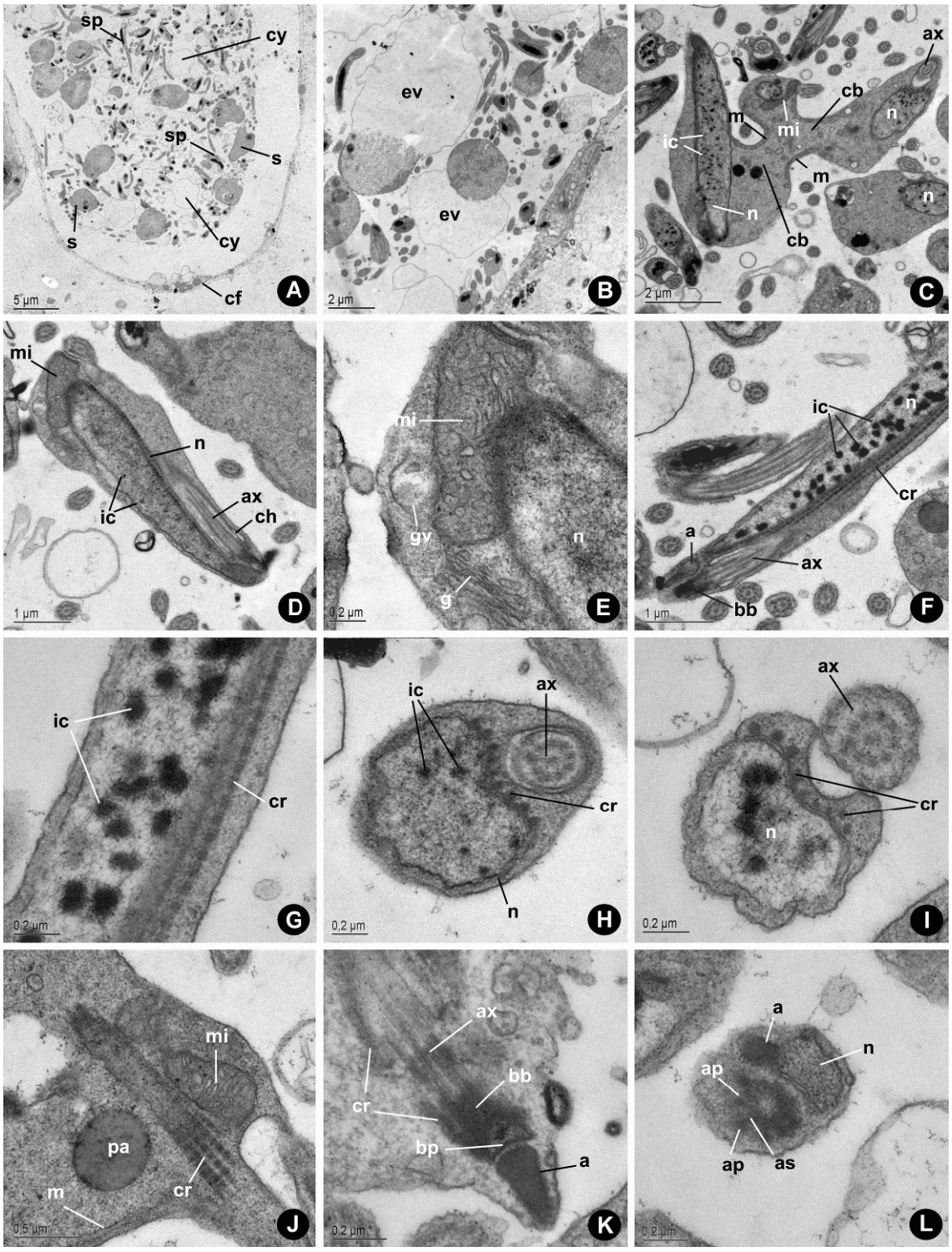
sp
cy
sp
s
s
cy
cf
5 µm
A
ev
ev
2 µm
B
ax
cb
m
mi
n
ic
m
n
n
cb
2 µm
C
mi
n
ic
ax
ch
1 µm
D
mi
gv
n
g
0,2 µm
E
ic
n
cr
a
ax
bb
1 µm
F
ic
cr
0,2 µm
G
ic
ax
cr
n
0,2 µm
H
ax
cr
n
0,2 µm
I
mi
pa
m
cr
0,5 µm
J
ax
bb
cr
bp
a
0,2 µm
K
a
n
ap
ap
as
0,2 µm
L

Formation of an electron-dense, membrane-bounded acrosome at the new functional anterior pole was completed (Fig. 6A, D-E). There was also an electron-dense acrosomal rod (Fig. 6D-E), which located between the acrosome and the nucleus, adjacent to the basal body. In some spermatozoa, a small vesicle, characterized by a six-layer membrane, surmounted the acrosome and protruded the cell membrane (Fig. 6D-E).

Figure 6. Mature spermatozoa. **(A)** Longitudinal section of a spermatozoon showing the helical arrangement of the chromatin in the nucleus (n), the acrosome (a), the acrosomal rod (ar), the basal body (bb), and the cytoplasmic tunnel (ct). **(B)** Cross section of a spermatozoon showing the axoneme (ax) within the cytoplasmic tunnel. Note the typical 9+2 organization of the axoneme. **(C)** Longitudinal section of a spermatozoon showing the nuclear ends (n), the tail insertion within the cytoplasmic tunnel (ct), and the tendency of the axoneme (ax) to cross the longitudinal axis of the cell body (see Fig. 7a). Long striated rootlets (cr) and the single mitochondrion (mi) are also patent. **(D)** Longitudinal section at the acrosomal cell pole showing the cytoplasmic tunnel (ct) lodging insertion of the axoneme (ax), a conical acrosome (a) located adjacent to the acrosomal rod (ar) and the basal body (bb). **(E-F)** Detail of the conical acrosome (a) and the acrosomal rod (ar). A vesicle (av) characterized by a complex, multilayered membrane surmounts the acrosome.

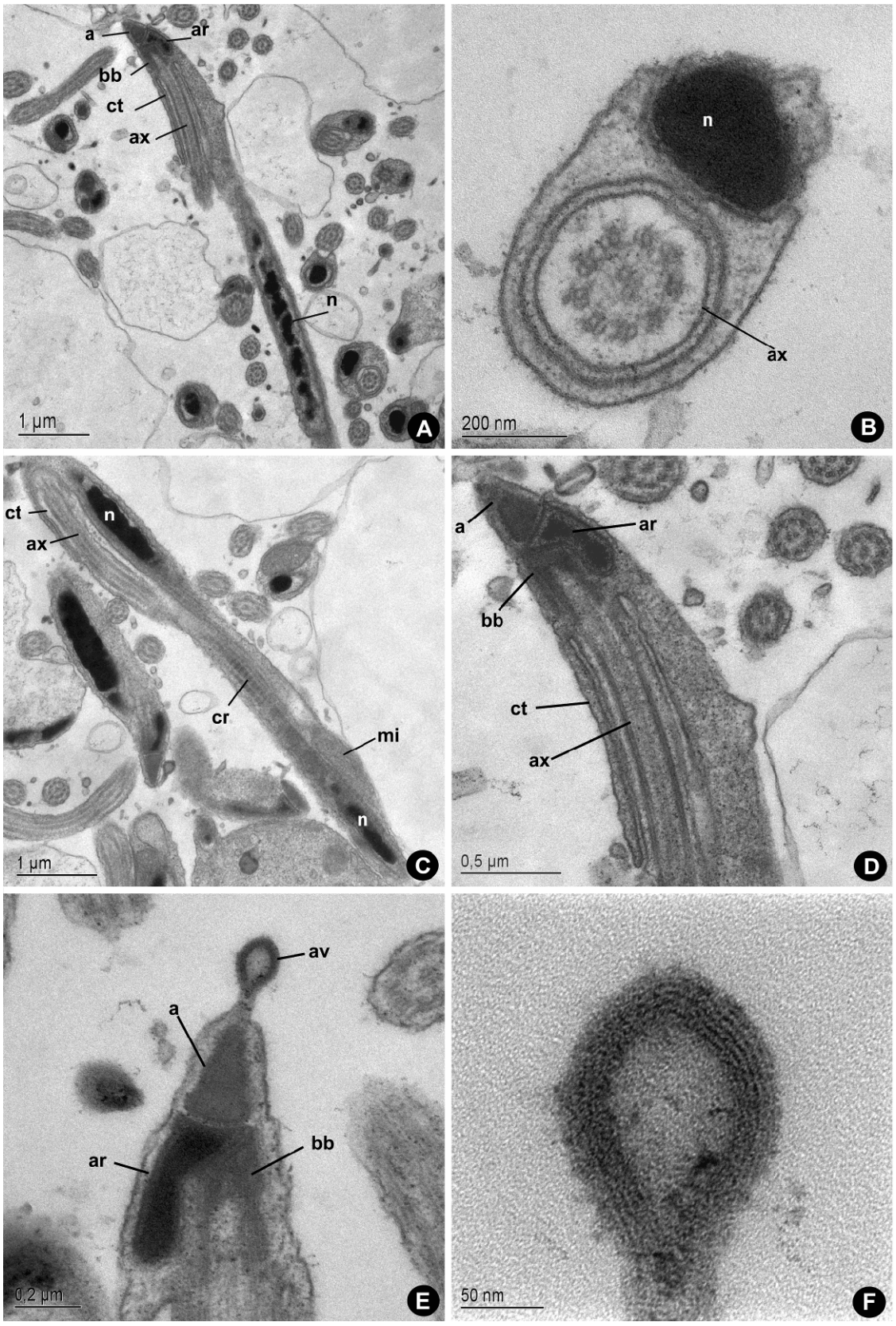
a
ar
bb
ct
ax
n
1 µm
A
n
ax
200 nm
B
ct
n
ax
cr
mi
n
1 µm
C
a
ar
bb
ct
ax
0,5 µm
D
av
a
bb
ar
0,2 µm
E
50 nm
F

Discussion

Spermatogenesis in *Crambe crambe* unfolds throughout early stages (i.e., spermatogonia, primary and secondary spermatocytes) that closely follow the pattern observed in most other demosponges (e.g., Fell 1974; Simpson 1984; Harrison and De Vos 1991; Boury-Esnault and Jamieson 1999; Riesgo et al. 2007), including the derivation of flagellated spermatogonia from choanocytes. Nevertheless, ever since the secondary spermatocyte, the process strongly departs from what it would be expected to occur not only in demosponges but also in other lower metazoans. At the spermatid stage, the formation of a deep ciliary pit to harbor the flagellum insertion and a long portion of the proximal axoneme produces a V-shaped sperm similar in general organization to that known in some phoronids (Fig. 7e; e.g., Franzén and Ahlfors 1980; Zimmer 1991; Reunov and Klepal 2004). While it has been suggested that such a cytoplasmic tunnel is formed in *Phoronopsis harmeri* by migration of the ciliary basal body from the posterior to the anterior cell pole (Reunov and Klepal 2004), our observations suggest that it rather forms in *C. crambe* because the cytoplasm stretches around the proximal portion of the flagellum. It is also worth noting that, in addition to *C. crambe*, several spongillids, such as *L. baikalensis* (Efremova and Parkovskaya 1980), *E. fluviatilis*, and *Spongilla lacustris* (Paulus 1989), do also posses a relatively deep cytoplasmic pit (Fig. 7C-D). None of these sponges show V-shaped sperm. Nevertheless, given the relative scarcity of information regarding spermatogenesis and sperms in the Porifera and the deep ciliary pit found in spermatids of the poecilosclerid demosponge *Anchinoe paupertas* -whose mature spermatozoon remains uninvestigated (De Vos et al. 1991), it cannot be rule out that V-shaped spermatozoa may occur more often than thought in some poecilosclerid subgroups. Interestingly, a V-shaped spermatozoon, but lacking cytoplasmic tunneling for the tail (Fig. 7B), occurs in the halichondriid demosponge *Halichondria panicea* (Barthel and Detmer 1990).

In association with the flagellum, we have found well-developed striated rootlets that originate from the basal body and run parallel to the nuclear envelope to reach the mitochondrion located at the opposite cell pole. Such structures had never been reported

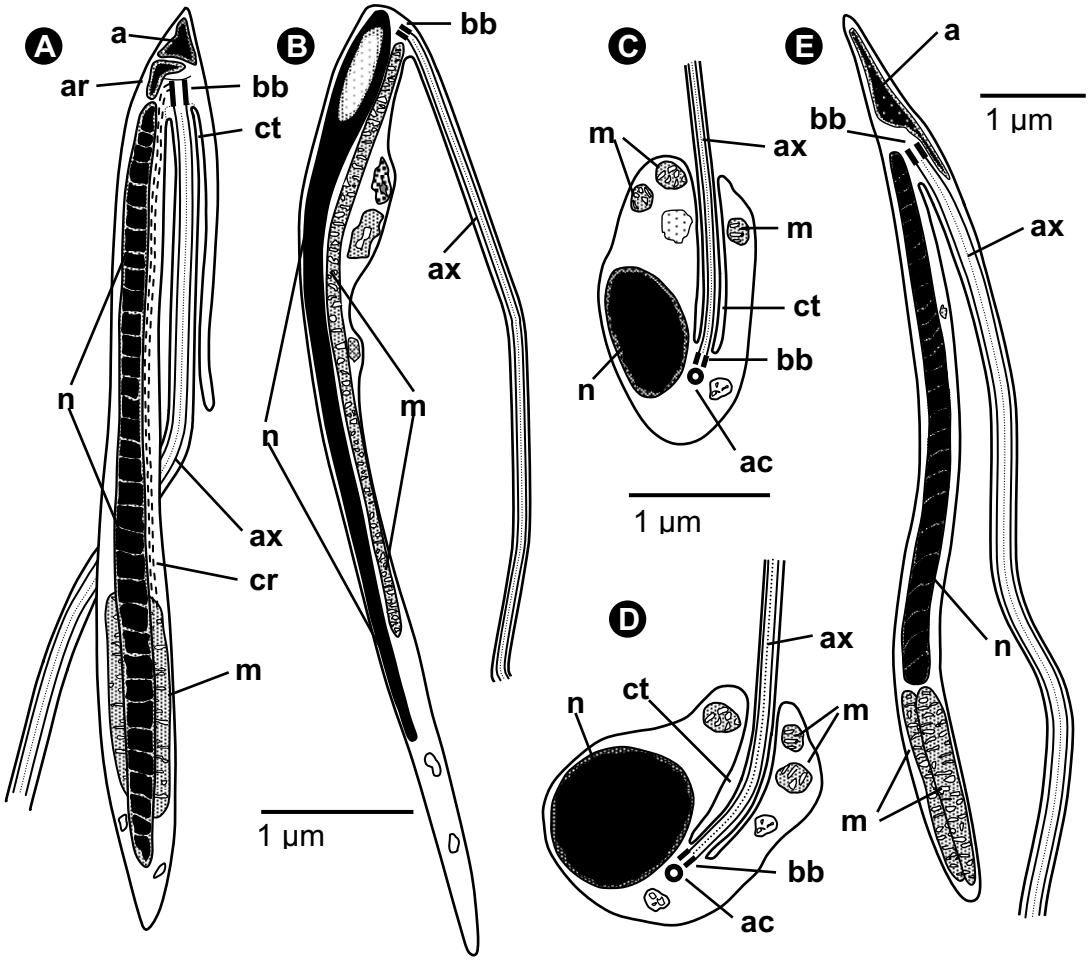

Figure 7. Schematic diagram summarizing the ultrastructure of several demospongian sperms and the spermatozoon of the phoronid *Phoronopsis harmeri* **(A)** V-shaped spermatozoon of the poecilosclerid Crambe crambe. **(B)** V-shaped sperm of the halichondriid *Halichondria panicea* (modified from Barthel and Detmer 1990). **(C-D)** Spermatozoan of the haplosclerid *Spongilla lacustris* (modified from Paulus 1989) and *Lubomirskia baikalensis* (modified from Efremova and Parkovskaya 1980). **(E)** V-shaped spermatozoon of the phoronid *P. harmeri* (modified from Reunov and Klepal 2004). Codes: a, acrosome; ac, accessory centriole; ar, acrosomal rod; ax, axoneme; bb, basal body; ct, cytoplasmic tunnel; cr, ciliary rootlets; m, mitochondrion; n, nucleus.

in the sperm of other poriferans to date. The striated rootlets of *Crambe crambe* could have a role in reinforcing the anchoring of the flagellum, which may require extra-support when pushing the V-shaped cell. Nevertheless, they may also participate in

transferring the energy from the mitochondrion to the basal body for ciliary beating, since large mitochondria usually occur in contact with rootlets in many types of flagellum-bearing cells in sponges (e.g., Woollacott and Pinto 1995; Maldonado et al. 2003; Maldonado 2004).

Other remarkable transformation during spermiogenesis of *Crambe crambe* is that spermatids elongate substantially, their nucleus stretches accordingly, and its chromatin condenses by a multipolar process into a helical structure. Helically-condensed chromatin is known from the modified sperm of some invertebrates, such as phoronids (e.g., Reunov and Klepal 2004) and octopodan cephalopod mollusks (e.g., Diaspro et al. 1997; Giménez-Bonafé et al. 2002), and it should not be confused with helical coiling of an elongated nucleus, as reported in sperms of gastrotrichs (Ferraguti and Balsamo 1995), oligochaetes (Erséus and Ferraguti 1995), chelicerates (Alberti 1995), etc. Immediately prior to nuclear elongation of *C. crambe* spermatids, tube-like structures (Fig. 4E-F) appear attached to the internal side of the nuclear envelope. We suspect that these structures may be microtubule-derived and somehow involved in the process of nuclear stretching. Cytoplasmic microtubules have occasionally been regarded to be involved in stretching and helicoidally coiling of the sperm nucleus in other invertebrates (e.g., Diaspro et al. 1997; Gimenez-Bonafé et al. 2002). Microtubules also occurred reinforcing the internal side of the plasmalemma in the inter-spermatid bridges (Fig. 5C, J). Similar structures had never been described during the spermatogenesis of the Porifera.

The presence of a subacrosomal rod in *Crambe crambe*, which according to its appearance and position appear to be homologous to the axial rod (= perforatorium) known from the sperms of most invertebrates and vertebrate animals, is also noteworthy. To date ctenophores and nemerteans were thought to be the lowest metazoan groups possessing a well-developed acrosome with subacrosomal rod (Franzén 1987). Although the axial rod of spermatozooa was originally regarded as a structure designed to pierce the egg membranes mechanically, the modern view is that this proteinaceous structure is a cytoskeletal piece that anchors the proximal region of the acrosome to the nuclear membrane below. To date no other sponge spermatozoon had been reported to have a subacrosomal rod. Another unprecedented feature is the small vesicle, characterized by a multilayer-layer membrane that surmounts the acrosome (Fig. 6 D-E).

Our ultrastructural findings are largely consistent with the brief but excellent study by Tripepi et al. (1984), in which many of the striking features of the sperm of *Crambe crambe* were formerly outlined. A discrepancy are the 2 electron-dense "basal rods" of unknown function, which along with the mitochondrion were reported to flank the nucleus, and have not been found in our study.

Unlike expressed in most general reviews on the evolution of animal sperm, the available information to date clearly indicates that the sperms of demosponges can be classified as belonging to 2 structural types, i.e., "primitive" and "modified" (sensu Reunov 2005), depending on taxa. Such a situation is similar to that known in many protostomes (e.g., Afzelius 1979; Ying et al. 2004) and a few deuterostome groups (e.g., Afzelius 1971). The evolutionary significance of this fact regarding the Porifera is intriguing. Because V-shaped and elongated spermatozoa with elongated nucleus are widely regarded as a sperms of the "modified" type (e.g., Franzén 1987, Reunov 2005), one should conclude that co-occurrence of "primitive" and "modified" sperms is the ancestral condition in the Porifera, hence pre-dating the apparition of higher metazoans. On the other hand, it is long postulated that the shape of the sperm cell is influenced by not only phylogenetic relationships but also physiological and functional demands during dispersal and fertilization (e.g., Franzén 1956; Afzelius 1979; Rouse and Jamieson 1987). From this perspective, the spermatozoon of *Crambe crambe*, which is a hermaphroditic sperm-casting demosponge, belongs to the "entaquaspermatozoon" type, i.e., modified sperm that is first released to the seawater by a male-acting individual and subsequently taken by female-acting conspecifics (Rouse and Jamieson 1987). At first sight, functional demands cannot easily be invoked to account for the distinctive morphology of the spermatozoon of *C. crambe* relative to that of other sperm-casting demosponges. Internal fertilization in *C. crambe* is thought to follow a process similar to that occurring in many other brooding demosponges, which, however, posses the classical, primitive sperm. In these sperm-casting, internally-fertilizing demosponges, the sequence of events leading to the transference of the spermatozoon to the oocyte cytoplasm can be summarized in 3 steps: 1) choanocytes of the female-acting individuals engulf free-swimming spermatozoan that entered the body with the inhalant seawater flow; 2) these choanocytes disassemble their flagellum and the collar microvilli and leave the choanochambers as amoeboid cells (i.e., carrier cells), carrying the spermatozoon within a non-digestive vacuole, the spermiocyst; 3) carrier cells find oocytes nested in the dense collagen mesenchyme (the mesohyl) and fuse their

plasmalemma with the oolemma, transferring the spermiocyst to the oocyte cytoplasm. Such a fertilization process is unique among Metazoa.

Internal fertilization in *Crambe crambe* has been assumed -though never confirmed- to follow the above-outlined, general pattern (i.e., carrier-cell transmission), which is thought to take place in all brooding demosponges. Nevertheless, a glance to the scientific literature reveals that the participation of carrier cells is well documented in fertilization of sponges belonging to the class Calcarea only (e.g., Simpson 1984; Harrison and De Vos 1991; Nakamura et al. 1998). Surprisingly, although spongiologists have widely assumed that internal fertilization in Demospongiae is mediated by carrier cells as well, no TEM study has corroborated this issue to date. If no carrier cell would act in the transmission of the spermatozoon to the oocyte, the "V" shape could be interpreted as a morphological design addressed to enhance sperm movement through the mesohyl, a collagen-rich medium far more viscous than seawater. A spermatozoon attempting to swim forward in such a dense medium would require enhanced rotation capabilities to deal with viscosity. We postulate that the reason why the proximal portion of the axoneme does not run parallel to the longitudinal axis of the sperm head but crosses it (Fig. 7A) -as it was also depicted by Tripepi *et al.* (1984)-, is that such an arrangement favors rotation of the whole V-shaped sperm when moving forward. The short arm of the V-shaped structure, i.e., the sperm head, appears to be designed to stabilize the gravity center during rotation, counterbalancing the pushing of the tail. Likewise, if no carrier cell would be involved in sperm transfer, the presence of a complex acrosomal system to enter the oocyte would be justified. Therefore, if we are to understand the biological significance of the V-shaped sperm of *Crambe crambe*, it will be crucial to observe free-swimming spermatozoa and elucidate whether internal fertilization is mediated by carried cells or an alternative, unknown mechanism.